NONLINEAR COMPRESSIVE BEHAVIOR OF ADJACENT COLD FORMED STEEL LIPPED CHANNEL SECTIONS

Md. Abdul Basit[*1], Ishtiaque Ahmed[2] and Mohammad Anwar-Us-Saadat[3]

[1] *Assistant Professor, International University of Business Agriculture and Technology, Bangladesh, e-mail: abdul.basit@iubat.edu*
[2] *Professor, Bangladesh University of Engineering and Technology, Bangladesh, e-mail: iahmed87@gmail.com*
[3] *Lecturer, Melbourne Polytechnic, Australia, e-mail: mausaadat@melbournepolytechnic.edu.au*

***Corresponding Author**

ABSTRACT

Usage of accumulated Cold Formed Steel (CFS) members as construction material are increasing as CFS members offer various benefits, such as being lightweight, fewer long-term maintenance needed due to durability and not requiring formwork etc. Some degree of published research has been reported that explored how the axial compression-resistant strength and stability of such channels are affected by the width-to-thickness ratio (b/t) and lip height-to-thickness ratio (c/t). Besides, current design codes like Eurocode (EC), American Iron and Steel Institute (AISI) and the Australian and New Zealand standards (AS/NZ) consist of inadequate guidance on the approximation of strength of built-up CFS columns in view of different width-to-thickness ratio and lip height-to-thickness ratio. This research represents a numerical analysis of the performance shown by built-up CFS lipped sections taking varying width-to-thickness (b/t) ratios and lip height-to-thickness (c/t) ratios of dissimilar columns. Nonlinear Finite Element Model (FEM) was analyzed built on previous thirty investigational findings taking into account various substantial models and geometric imperfections. Axially loaded compressive strengths computed from FEM displays strong agreement with practical results from earlier studies confirming the model's reliability. After that, a parametric study including over-all eighty-eight models were conducted using all the ideologies of verified model concepts, with varying (b/t) and (c/t) ratios and covering a wide range of column lengths (stub, short, intermediate and slender) which has produced enough data on the maximum axial force of such channels. Attained column strengths were compared with the design strengths calculated in accordance with the AISI standard. For all four types of columns, it was found that the AISI standard had forecasted slight increased strength values in comparison to finite element results in the majority of situations. From the comparison results, some design curves were also created that can be used to predict the buckling behavior of these channels.

Keywords: *Lipped channels, finite element modelling, cold formed steel, built up section, pure compression*

1. INTRODUCTION

Using structural sheet steel that has been cut to C-sections and additionally formed by rolling the steel over a sequence of dies, CFS members are created. A variety of steel thicknesses are available for structural as well as non-structural roles (build steel.org). In both residential and commercial buildings, practice of built-up CFS members is growing because they are lightweight and simple to construct into the desired shape (Darcy and Mahendran, 2008). In steel trusses, CFS lipped channels are employed as a compression component; however, in portal frames, they are used as columns (Lawson et al., 2008). The separate channels in this cross-section are prevented from buckling by lengthwise ties at specific positions (Ting et al., 2018). The design codes provide insufficient instruction for estimating the strength of built-up CFS channels (Kechidi et al., 2020).

For this type of channels under compression, some research has been done. (Ting et al., 2018) has investigated the way that adjacent built-up CFS lipped sections behave exposed to axial compression using both numerical and experimental methods. The results of thirty experiments are described performed on these sections starting with stub and finishing with slender columns. For expanding the research, (Roy et al., 2018) has checked out the impact of thickness on the performance of these channels. The axial strength of back-to-back gapped CFS lipped channels was also examined experimentally and numerically by (Roy et al., 2018, Roy et al., 2018) who also came to the conclusion that the present design standards provided by (AISI, 2016) and AS/NZ code (Standards Australia, 2005) may be overly conventional when calculating the axial strength of that type of columns. Furthermore, (Roy et al., 2018) recently performed research on two CFS channels that had been built up back to back. These experimental findings supported the numerical FEM (Roy et al., 2018). Additionally, (Roy et al., 2018) looked into the nonlinear behavior of axially loaded back-to-back cold-formed stainless steel channels and came to the conclusion that no prior research had looked at back-to-back cold-formed un-lipped channels or specifically examined the impact of spacing of screw on their axial strength. (Fratamico et al., 2016) looked at how screw spacing affected the response of adjacent built-up lipped columns. Thirty columns were modeled in his study under concentric loading conditions all the way to failure. Results revealed two typical deformation modes. (Stone and Laboube, 2005) considered the identical channels, but they featured strengthened track portions and flanges. Based on the findings of the inquiry, it was determined that the current design specifications were cautious when determining the maximum strength of built-up columns. (Zhang and Young, 2012) looked at the same sections with an opening. CFS built-up closed sections with discontinuous stiffeners were looked into by (Young and Chen, 2008). It is demonstrated that when obtaining buckling stresses for a single section, Direct Strength Method (DSM) is typically conservative. (Anbarasu and Ashraf, 2016) looked on the structural act of cold-formed, lean duplex stainless steel, single-lipped columns. The measured strengths were compared to those calculated using both the modified DSM suggested by (Becque et al., 2008) and the primary DSM established for CFS. The comparison showed that when calculating the strengths of the lipped channels, both the main and modified DSM techniques were incredibly conservative.

(Anbarasu et al., 2015) looked into the effectiveness and durability of built-up batten columns with CFS web stiffening. A recommendation has been made to alter the current DSM for calculating the axial capacity of that type of column. The column strength predicted by FEM is equated with the design column strengths predicted by the DSM. (Dabaon et al., 2015) researched built-up battened columns and came to the conclusion that when steel battened columns failed owing to flexural buckling, AISI and Eurocode standards were cautious; but when they failed due to local buckling, they were unconservative. (Whittle and Ramseyer, 2009) considered toe to toe welded built-up sections. According to reports, strengths based on the unmodified slenderness ratio and screw requirements were typically controlled while use of the modified slenderness ratio was exceptionally cautious. (Piyawat et al., 2013) examined back-to-back channel sections with welded lipped edges. The proposed equation in this research for the axial load capacity showed fair agreement with the capabilities that were both computationally simulated and experimentally verified. (Aslani and Goel, 1991) investigated an interpretive criterion for built-up compression members buckling strength. (Reyes and Guzman, 2011) completed related study and they evaluated the slenderness ratio in built-

up cold formed box sections, Additionally, (Biggs et al., 2015) demonstrated that for wider members (AISI, 2016) can be cautious and for broader members, it can be less conservative.

Hence, it can be said that only a small amount of research has examined the impact of (b/t) and (c/t) on the capacity of this type of channels when subjected to compression axially (Roy et al., 2019), which necessitates further study in this area. This work makes an effort to evaluate how different (b/t) ratios and (c/t) ratios affect the axial compressive strength of lipped channels of various lengths (stub, short, intermediate and slender). The outcomes of the parametric analysis were related with computed design strengths in line with the AISI regulation.

2. DESIGN GUIDELINES IN LINE WITH AISI, BNBC AND AS/NZ STANDARD

In this section the design guidelines from American Iron and Steel Institute (AISI) specification (AISI, 2016) for cross section and member design will be presented. The design steps include determination of effective width area first based on the (b/t) ratio, depth-to-thickness ratio (d/t) and design strengths as stated by AISI, which complies with AS/NZ standard and which also said to be followed in Bangladesh National Building Code (BNBC).
According to AISI and AS/NZ standard, the un-factored design strength of axially loaded columns for built-up lipped channel sections is as follows

$$P_{AISI\ \&\ AUS/NZ} = A_g F_n \quad (1)$$

Here A_g = *gross area*

Critical buckling stress F_n is calculated as

For $\lambda_c \leq 1.5$

$$F_n = (0.658^{\lambda_c^2})\, F_y \quad (2)$$

For $\lambda_c > 1.5$

$$F_n = (\frac{0.877}{\lambda_c^2})\, F_y \quad (3)$$

Calculation of non-dimensional slenderness (λ_c) will be

$$\lambda_c = \sqrt{\frac{F_y}{F_e}} \quad (4)$$

F_e = Elastic global buckling stress = $\frac{\pi^2 E}{(\frac{KL}{r})^2}$ (5)

L= length of column, K= effective length factor,
Modified slenderness ratio for compression members composed of back-to-back sections in touch was calculated as

$$(\frac{KL}{r})_m = \sqrt{(\frac{KL}{r})_0^{\ 2} + (\frac{a}{r_i})^2} \quad (6)$$

$\frac{a}{r_i}$ does not surpass half of the controlling slenderness ratio
Where $(\frac{KL}{r})_0$ = total slenderness ratio of entire section
a = distance between intermediate fastener
r_i =lowest radius of gyration of entire area

3. SUMMARY OF EXPERIMENTAL RESEARCH (TING ET AL., 2018)

FEM were created and tested against the experimental program done by (Ting et al., 2018) on back-to-back built-up lipped channels under compression in the current study. These cross-sections were created by adjoining two lipped channel sections at their web by means of screws. Figure 1 presents a typical cross-section detail of the members used within the experimental program. A total of 30 specimens were evaluated. Summary of the specimen details are given in Table 2. Where BU-75 stands for built-up back-to-back channel-sections with 75 mm web depth, S = tied joint spacing and 1,2,3 are representing 1st, 2nd and 3rd specimen respectively.

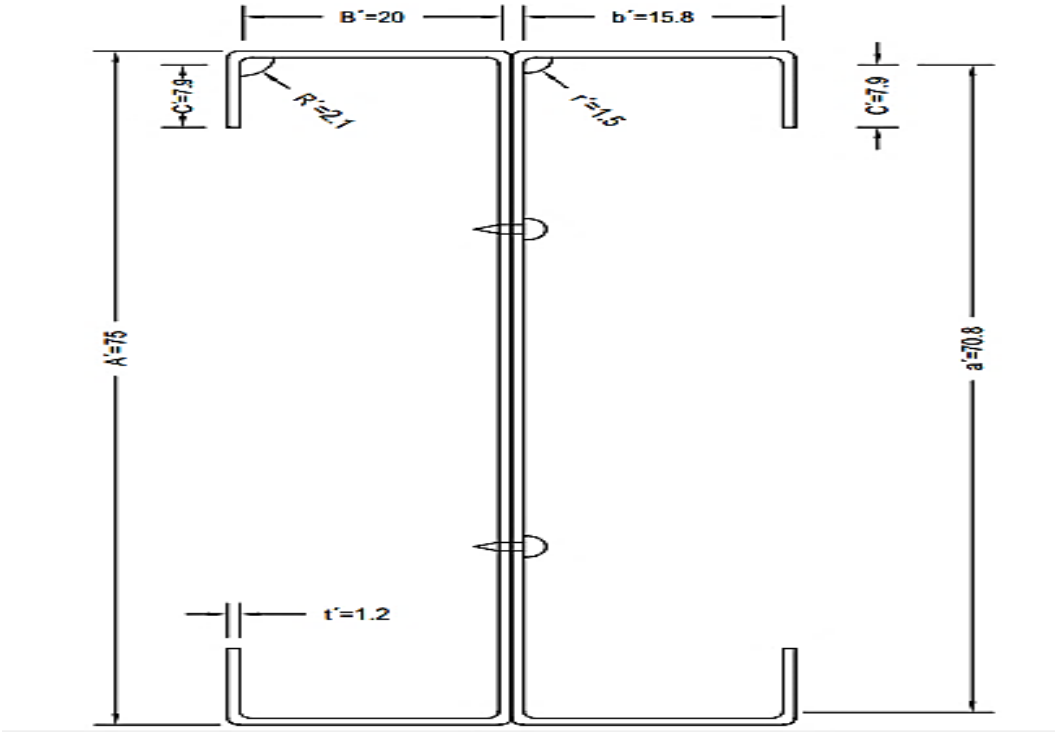

Figure 1: Specifications of two adjacent cold-formed steel channel sections (Ting et al., 2018)

4. NUMERICAL RESEARCH

4.1 General

FEM of built-up lipped channels were created using non-linear elastic-plastic approach by (ABAQUS 6.13-1). Consequently, strengths generated from these models were compared and validated against the experimental test outcomes received by (Ting et al., 2018) in order to confirm the applicability of the modelling principles for further parametric studies on similar cross-sections. FEM were analyzed twice, firstly an eigenvalue analysis then followed by a nonlinear analysis. The linear elastic eigenvalue analysis is used to get the shape of the initial imperfections. Based on the deformed shape obtained from eigenvalue analysis, initial geometric imperfection was imposed on the member prior to the nonlinear analysis. Using the static riks method from the ABAQUS library, the load displacement nonlinear analysis was performed. The geometric imperfections (local and global) and material nonlinearity were accounted within the FEM. The next sections go into greater detail on the modelling methodologies.

4.2 Geometry and material properties

The whole geometry of the steel lipped channels was developed based on the information obtained from the experimental program. ABAQUS requires input of material strength in its material property section in the form of real stress and log plastic strain. In this modeling, there were two different types of material properties. First, the Von Mises yield concept was employed to create a graph of simple elastic perfect plastic stress-strain. A different kind of material model that incorporates the full range stress-strain curve provided by (Gardner and Yun, 2018) for cold-formed steel is also used. Inclusion of both techniques helped to understand the effect of using different techniques within the material model. Modeling employed yield stresses of 560 MPa and ultimate stress of 690 MPa with a Young's modulus of 207 GPa (Roy et al., 2018). Poisson's ratio of steel was taken as 0.3. This numerical model combined appropriate material strength, including increased corner strength data for elements in corner zones and flat material data for elements in flat zones. According to (Gardner et al., 2010) for CFS, the increase in corner strength was carried into the flat zone for a distance equal to the section thickness t. Figure 2 depicts the nonlinear material property that has been used in ABAQUS.

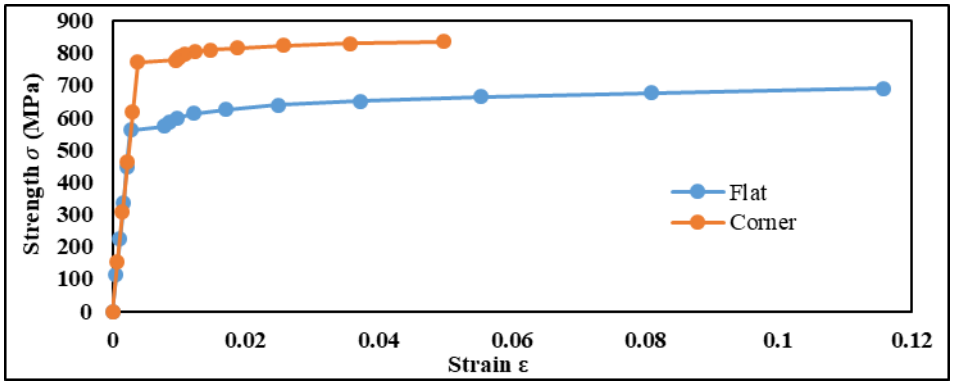

Figure 2: Stress-strain curve developed for different regions

4.3 Mesh optimization

From ABAQUS mesh library, to model the section, a linear 4-noded quadrilateral shell section (S4R5) with reduced integration that is reported in (Anwar et al., 2016) as suited for thin-walled metallic cross sections was chosen. For the model convergence, a square mesh that is constant measuring 5 mm by 5 mm (length by breadth) was used. The suitability of this mesh size is shown in Table 1 and Figure 3. The quantity of elements was elected lengthwise of the sections to maintain a roughly one-to-one aspect ratio for all the parts. Two elements were present at the corner which was determined to be the ideal quantity for consistent meshing.

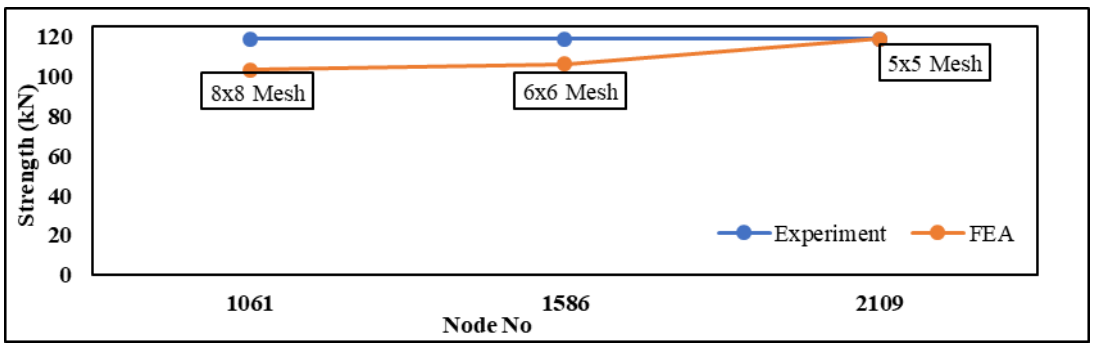

Figure 3: Comparison between FEM and experimental strength for various mesh sizes

Table 1: Investigation of mesh convergence

Type of Mesh	Element size at flat (mm × mm)	Total element in corner	Total elements	Total nodes

Fine	5×5	2	2016	2109
Medium	6×6	2	1513	1530
Coarse	8×8	2	1000	1023

4.4 Boundary settings, constraints and application of load

Stub columns had their ends restrained from any movement other than the loaded end, which was permitted against translation in the direction of the load. Pin-ended boundary settings for other columns were used. Rotation was permitted at both the top and bottom of the built-up channels through reference points in order to assign pin-ended boundary conditions. The built-up channel cross section center of gravity (CG) was chosen as the reference point and eccentricity was not taken into consideration. At the top end of the channels, the load was assigned to the point of reference. The physical equivalent of a screw, known as a node to node tied joint, was utilized to connect the webs of two back-to-back built up lipped channels. The tied joint was positioned h/4 from the top and bottom as shown in Figure 4 (where h is the height of the web). Using the rigid body constraint option, the end nodes were mounted on the top and bottom reference points in order to prevent any form of movement at the ends. Screws were used in the actual experimental program in order to ensure the joint between the lipped channels. In order to simplify the FEM, instead of screws node to node tied joints at channel webs were used. Key assumption for using the node to node tied joint in lieu of screwed joint was considering the screws hold the lipped channels tightly together in a way, that the channels will not have any relative translational or rotational movement, rather act as one at the locations where the screws were placed. Number of tied joints depended on the number of screws used in the actual specimen.

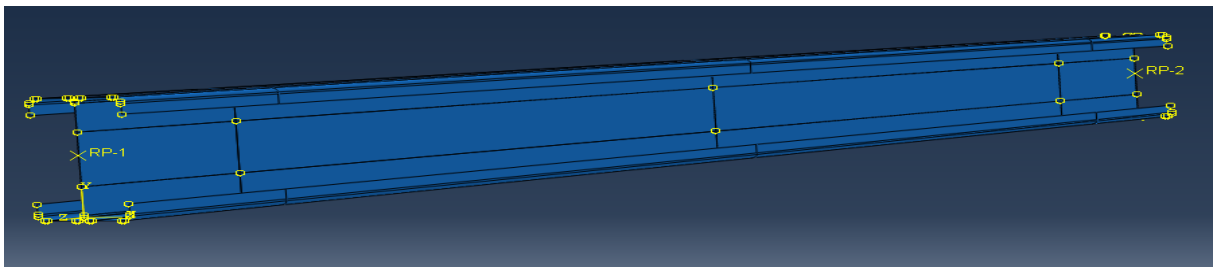

Figure 4: Rigid body constraint and tied joint utilized in FEM

4.5 Contact modelling among the channels

"Surface to surface" contact was employed by means of finite-sliding tracking method to create the connection in between webs of adjacent lipped channels. One lipped channels web worked as master surface whereas the slave surface was thought to be the other lipped channel web. As like (Kechidi et al., 2020) with a coefficient of friction of 0.19 for steel to steel, the penalty friction system was utilized to imprecise the performance of intense pressure over closure.

4.6 Modelling of local and global geometric imperfections

Local and overall buckling actions of built-up sections depend on a variety of characteristics like (b/t) ratio, (d/t) ratio etc. (Roy et al., 2018). Imperfection of the real specimen is an obvious feature which intrigues the final failure mode and strength. Thus, it is crucial to examine the effect of initial imperfection within the FEM. While incorporating the initial imperfection within the FEM there are two factors to be considered (1) shape of the model and (2) amplitude of the shape. The shape of the imperfection specimen could be obtained from the actual specimen or could be replicated using the warped shapes generated from elastic buckling analysis. The later approach is widely used by the prior researchers and also adopted in the current research. The imperfection contours for the stub, short, intermediate and slender columns are shown in Figure 5. The shape of the imperfection was determined by the lowest eigen mode. Amplitude of the imperfect specimen refers to the magnitude of the maximum distortion in length units compared to the ideal cross-section and length wise geometry. The impacts of early imperfections on compressive behavior were examined using four dissimilar

amplitudes: Dawson-Walker model for CFS (Gardner and Nethercot, 2004), t/100, t/10 and 0.5% of t. Four distinct amplitudes as L/1000, L/100, L/200 and L/300 were chosen for global imperfections. For stub and short columns, only local imperfections, for slender columns only global imperfections and for intermediate columns. local as well as global imperfections were taken into account.

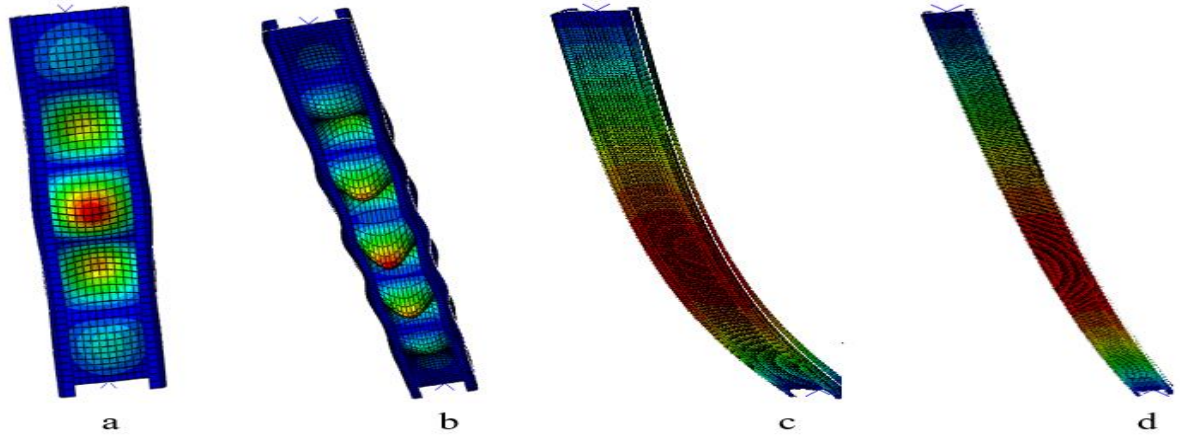

Figure 5: Initial imperfection contours for all columns (a) Stub (b) Short (c) Intermediate (d) Slender

4.7 Finite element model validation using experimental findings

The FEM established in this research based on aforementioned principles for CFS lipped channels were compared against the test results reported by (Ting et al., 2018). Key comparisons were made with the maximum load capacity, the load-deformation behavior and deformation shape between the actual sample and FEM. While the shape comparisons are illustrated in Figure 6, the strength comparison is presented in Table 2 and load-deformation behavior is shown in Figure 7.

Table 2: Assessment of the strength anticipated by the outcomes of the experiments (Ting et al., 2018) and the current model

Specimen Id	F_{EXP} (kN)	F_{FEM} (kN)	F_{EXP}/F_{FEM}
	Stub		
BU75-S50-L300-1	120.7	123.16	0.98
BU75-S50-L300-2	118.8	118.8	1.00
BU75-S50-L300-3	118.7	118.7	1.00
BU75-S100-L300-2	117.5	117.5	1.00
BU75-S100-L300-3	122.7	116.9	1.05
BU75-S100-L300-4	115.4	118.97	0.97
BU75-S200-L300-1	122.5	112.38	1.09
BU75-S200-L300-2	119.1	108.27	1.10
BU75-S200-L300-3	113.1	113	1.00
	Short		
BU75-S100-L500-1	83	96.51	0.86
BU75-S100-L500-3	74.1	93.8	0.79
BU75-S200-L500-1	86.2	95.78	0.9
BU75-S200-L500-2	88.9	91.65	0.97
BU75-S200-L500-3	93.6	93.5	1.00
BU75-S400-L500-1	74.8	78.74	0.95
BU75-S400-L500-2	80.6	80.6	1.00
	Intermediate		
BU75-S225-L1000-1	47	43.93	1.07
BU75-S225-L1000-2	46.3	43.27	1.07
BU75-S450-L1000-1	50.4	42.35	1.19
BU75-S450-L1000-2	45	35.71	1.26

BU75-S450-L1000-3	41.8	36.99	1.13
BU75-S900-L1000-1	39.9	39.5	1.01
BU75-S900-L1000-2	33.7	32.09	1.05
BU75-S900-L1000-3	31.5	31.82	0.99
Slender			
BU75-S475-L2000-2	10.9	9.82	1.11
BU75-S475-L2000-3	10.8	9.82	1.10
BU75-S950-L2000-2	8.8	9.36	0.94
BU75-S950-L2000-3	8.6	10	0.86
BU75-S1900-L2000-2	7.6	8.35	0.91
BU75-S1900-L2000-3	7.5	9.15	0.82

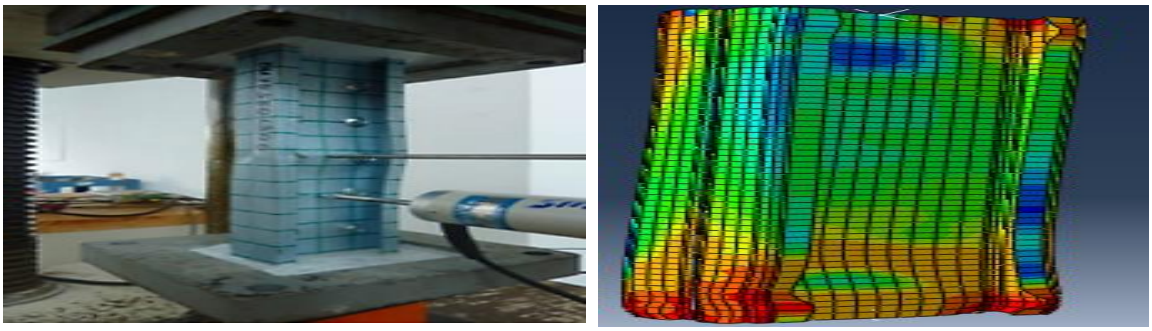

(a) Experimental (b) FEM

Figure 6: Experimental and FEM comparison of distorted shapes

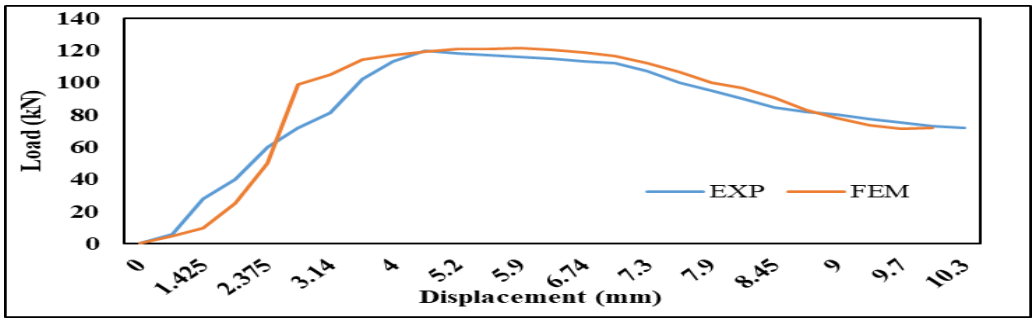

Figure 7: Comparison of load-displacement curve between experimental (Ting et al., 2018) and FEM

Two categories of material attributes are included in the numerical modeling for experimental verification [nonlinear entire stress strain graph, graph of simple stress strain] and for stub and short columns, there were 4 local imperfection amplitudes. For both forms of material modeling, two types of global imperfections were combined with three types of local imperfections for the intermediate column. Four different global imperfection categories were used for both types of material modeling on slender columns. Consequently, 272 numerical models were examined using experimental data from 30 specimens. The failure modes for the stub, short, intermediate and slender columns are depicted in Figure 8.

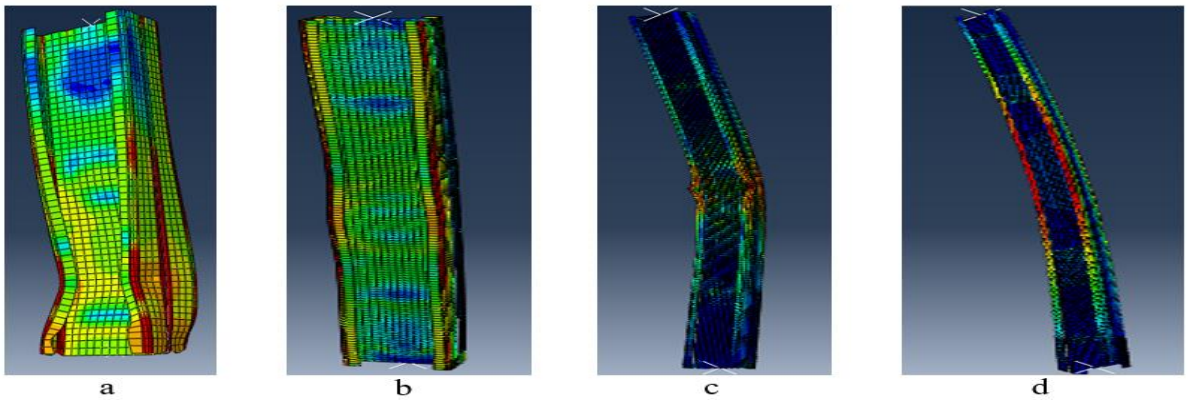

Figure 8: Failure pattern under axial force of all columns (a) stub (b) short (c) intermediate (d) slender

It is observed that the entire nonlinear stress-strain curve provides superior precision than the simplified elastic-plastic model. Local imperfection t/100 for stub and short columns, global imperfection L/1000 for slender columns and L/1000 as a global imperfection and t/10 as a local imperfection combinedly works as best for intermediate columns as proved by P_{EXP}/P_{FE} ratio.

5. PARAMETRIC STUDY

In the present research, with the intention of analyzing the impact of the (b/t) ratio and (c/t) ratio on the axial strength of back-to-back CFS lipped channels, a total of 88 distinct FEM was taken into consideration, each with a different section dimension and length (stub, short, intermediate and slender). Under both material model, for first four specimens, b/t ratio is taken according to the guideline given by EC and AISI and for the following two samples, the b/t ratio is taken beyond the limit. The c/t ratio for the final five specimens was determined in accordance with EC and AISI. Four different kinds of columns were taken into consideration in total starting with stub having a length of 300 mm, short (length of 700 mm), intermediate (length of 1200 mm) to slender (length of 2200 mm). There are two distinct material models employed. Full range stress strain curve was created regarding both kinds of material using the formula given by (Gardner & Yun 2018). Data on the yield strength and ultimate tensile strength of two commonly used steel grades have been gathered from a reputable Bangladeshi local steel manufacturer. The yield strength for material 1 is 345 MPa and the ultimate tensile strength is 450 MPa, while the yield strength for material 2 is 420 MPa and the ultimate tensile strength is 550 MPa. For both materials, a Poisson's ratio of 0.3 and an elasticity modulus of 200000 MPa are employed. Enhancements to corner strength have been made. There were total of 22 specimens modeled for each material for the four varieties of columns (stub, short, intermediate and slender). Figure 9 displays the failure mode of all columns.

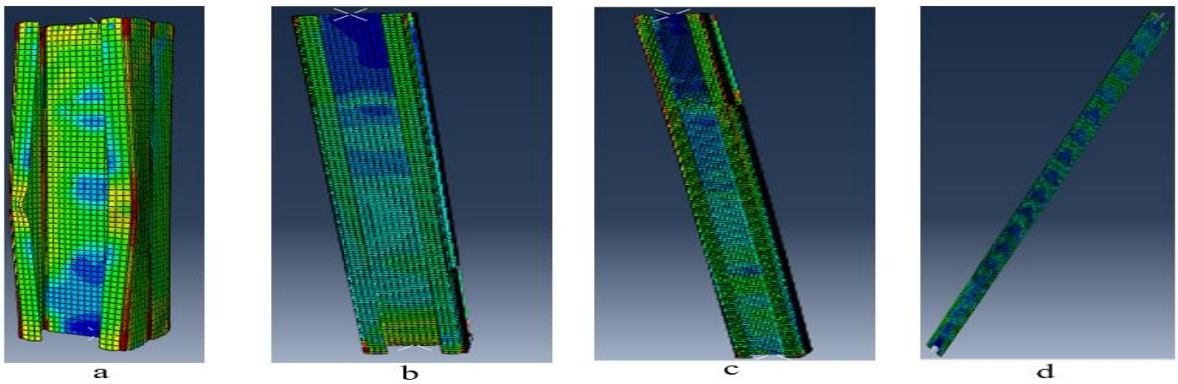

Figure 9: Von-Mises stress contour at maximum load for (a) stub (b) short (c) intermediate (d) slender

6. EVALUATING THE FINDINGS OF THE FEM AGAINST THE DESIGN STANDARDS

Strengths determined using AISI/AUS-NZ code and axial strengths derived from FEM are compared and presented in Table 3 to Table 10.

Table 3: Comparison of AISI design strength and FEM strength (stub-1)

Specimen	Web A (mm)	Flange B (mm)	Lip C (mm)	Thickness t (mm)	b/t	c/t	Spacing S (mm)	P_{FEM} kN	P_{AISI} kN	P_{FEM}/P_{AISI}
1	80	36	18	1.20	30	15	75	102.1	119	0.86
2	80	48	18	1.20	40	15	75	103.5	113.7	0.91
3	80	60	18	1.20	50	15	75	99.3	138.8	0.72
4	80	72	18	1.20	60	15	75	97.1	111.7	0.87
5	80	84	18	1.20	70	15	75	96.74	146.2	0.66
6	80	108	18	1.20	90	15	75	93.29	173.3	0.54
7	100	40	15	1.00	40	15	75	70.8	93.32	0.76
8	100	40	20	1.00	40	20	75	75.57	91.38	0.83
9	100	40	25	1.00	40	25	75	77.56	87.60	0.89
10	100	40	30	1.00	40	30	75	76.59	84.53	0.91
11	100	40	40	1.00	40	40	75	74.6	85.22	0.88
Avg.										**0.80**
COV										**0.17**

Table 4: Comparison of AISI design strength and FEM strength (stub-2)

Specimen	A	B	C	t	b/t	c/t	S	P_{FEA}	P_{AISI}	P_{FEM}/P_{AISI}
1	80	36	18	1.20	30	15	75	118.1	136.2	0.87
2	80	48	18	1.20	40	15	75	119.65	134.84	0.89
3	80	60	18	1.20	50	15	75	114.9	154.7	0.74
4	80	72	18	1.20	60	15	75	112.21	128.78	0.87
5	80	84	18	1.20	70	15	75	111.36	162.95	0.68
6	80	108	18	1.20	90	15	75	106.40	193.38	0.55
7	100	40	15	1.00	40	15	75	79.1	106.22	0.74
8	100	40	20	1.00	40	20	75	86.38	103.6	0.83
9	100	40	25	1.00	40	25	75	87.8	99.02	0.89
10	100	40	30	1.00	40	30	75	85.1	95.38	0.89
11	100	40	40	1.00	40	40	75	76.88	96.08	0.80
Avg.										**0.80**
COV										**0.15**

Table 5: Comparison of AISI design strength and FEM strength (short-1)

Specimen	A	B	C	t	b/t	c/t	S	P_{FEA}	P_{AISI}	P_{FEM}/P_{AISI}
1	80	36	18	1.20	30	15	175	102.35	111	0.92
2	80	48	18	1.20	40	15	175	103.57	109.69	0.94
3	80	60	18	1.20	50	15	175	101.2	135.98	0.75
4	80	72	18	1.20	60	15	175	92.07	110.33	0.83
5	80	84	18	1.20	70	15	175	83.9	135.7	0.62
6	80	108	18	1.20	90	15	175	77.2	172.4	0.45
7	100	40	15	1.00	40	15	175	72.06	86.57	0.83
8	100	40	20	1.00	40	20	175	74.03	85.69	0.86
9	100	40	25	1.00	40	25	175	78.54	82.79	0.95
10	100	40	30	1.00	40	30	175	76.80	80.3	0.96
11	100	40	40	1.00	40	40	175	64.1	81.49	0.79
Avg.										**0.81**
COV										**0.22**

Table 6: Comparison of AISI design strength and FEM strength (short-2)

Specimen	A	B	C	t	b/t	c/t	S	P_{FEA}	P_{AISI}	P_{FEM}/P_{AISI}
1	80	36	18	1.20	30	15	175	120.1	125.3	0.96
2	80	48	18	1.20	40	15	175	119.38	123.58	0.97
3	80	60	18	1.20	50	15	175	114.73	151.15	0.76
4	80	72	18	1.20	60	15	175	100.78	122.19	0.82
5	80	84	18	1.20	70	15	175	92.84	160.86	0.57
6	80	108	18	1.20	90	15	175	87.5	191.9	0.46
7	100	40	15	1.00	40	15	175	82.65	97.11	0.85
8	100	40	20	1.00	40	20	175	84.15	95.92	0.88
9	100	40	25	1.00	40	25	175	85.68	92.49	0.93
10	100	40	30	1.00	40	30	175	88.1	89.65	0.98
11	100	40	40	1.00	40	40	175	70.5	91.01	0.70
Avg.										**0.81**
COV										**0.24**

Table 7: Comparison of AISI design strength and FEM strength (intermediate-1)

Specimen	A	B	C	t	b/t	c/t	S	P_{FEA}	P_{AISI}	P_{FEM}/P_{AISI}
1	80	36	18	1.20	30	15	300	93.23	94.57	0.99
2	80	48	18	1.20	40	15	300	89.84	101.86	0.88
3	80	60	18	1.20	50	15	300	86.34	129.47	0.67
4	80	72	18	1.20	60	15	300	59.20	107.45	0.55
5	80	84	18	1.20	70	15	300	98.9	142.13	0.70
6	80	108	18	1.20	90	15	300	85.32	170.2	0.50
7	100	40	15	1.00	40	15	300	70.47	74.0	0.95
8	100	40	20	1.00	40	20	300	84.46	75.03	1.13
9	100	40	25	1.00	40	25	300	72.17	73.67	0.98
10	100	40	30	1.00	40	30	300	76.47	72.27	1.06
11	100	40	40	1.00	40	40	300	70.1	74.33	0.94
Avg.										**0.85**
COV										**0.28**

Table 8: Comparison of AISI design strength and FEM strength (intermediate-2)

Specimen	A	B	C	t	b/t	c/t	S	P_{FEA}	P_{AISI}	P_{FEM}/P_{AISI}
1	80	36	18	1.20	30	15	300	105.1	105.1	1.00
2	80	48	18	1.20	40	15	300	102.5	113.07	0.91
3	80	60	18	1.20	50	15	300	98.99	143.8	0.69
4	80	72	18	1.20	60	15	300	67.25	118.34	0.57
5	80	84	18	1.20	70	15	300	110.2	157.2	0.70
6	80	108	18	1.20	90	15	300	93.8	189.15	0.50
7	100	40	15	1.00	40	15	300	83.27	80.5	1.03
8	100	40	20	1.00	40	20	300	88.1	81.75	1.08
9	100	40	25	1.00	40	25	300	82.82	80.36	1.03
10	100	40	30	1.00	40	30	300	79.76	78.91	1.01
11	100	40	40	1.00	40	40	300	77.1	81.43	0.95
Avg.										**0.86**
COV										**0.27**

Table 9: Comparison of AISI design strength and FEM strength (slender-1)

Specimen	A	B	C	t	b/t	c/t	S	P_{FEA}	P_{AISI}	P_{FEM}/P_{AISI}
1	80	36	18	1.20	30	15	550	51.1	50.2	1.02
2	80	48	18	1.20	40	15	550	85.5	77.2	1.10
3	80	60	18	1.20	50	15	550	84.8	109	0.78
4	80	72	18	1.20	60	15	550	96.3	97.72	0.99
5	80	84	18	1.20	70	15	550	90.18	132.3	0.68

6	80	108	18	1.20	90	15	550	82.25	162.7	0.51
7	100	40	15	1.00	40	15	550	41.2	37.82	1.09
8	100	40	20	1.00	40	20	550	46.3	44.25	1.05
9	100	40	25	1.00	40	25	550	48.3	47.82	1.01
10	100	40	30	1.00	40	30	550	51.1	49.1	1.04
11	100	40	40	1.00	40	40	550	47.42	53.17	0.89
Avg.										**0.92**
COV										**0.23**

Table 10: Comparison of AISI design strength and FEM strength (slender-2)

Specimen	A	B	C	t	b/t	c/t	S	P_{FEA}	P_{AISI}	P_{FEM}/P_{AISI}
1	80	36	18	1.20	30	15	550	51.9	50.24	1.03
2	80	48	18	1.20	40	15	550	91.2	81.36	1.12
3	80	60	18	1.20	50	15	550	95.35	118.18	0.81
4	80	72	18	1.20	60	15	550	107	105.48	1.01
5	80	84	18	1.20	70	15	550	96.76	144.15	0.67
6	80	108	18	1.20	90	15	550	87.62	179.79	0.49
7	100	40	15	1.00	40	15	550	41.9	37.82	1.11
8	100	40	20	1.00	40	20	550	46.9	44.25	1.06
9	100	40	25	1.00	40	25	550	49.05	47.82	1.03
10	100	40	30	1.00	40	30	550	51.79	49.37	1.05
11	100	40	40	1.00	40	40	550	49.98	54.27	0.92
Avg.										**0.94**
COV										**0.24**

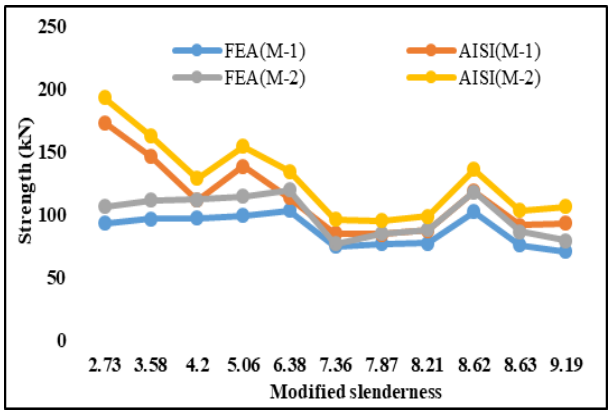

(a)

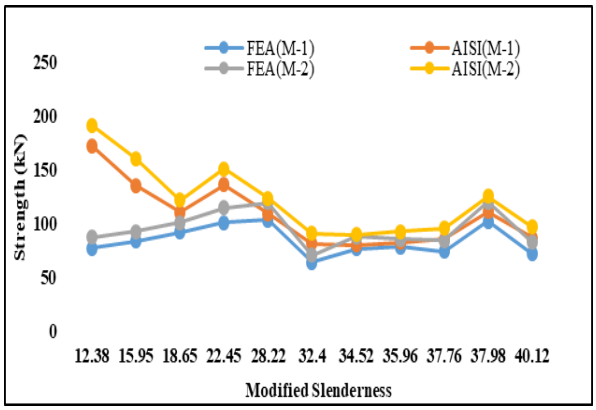

(b)

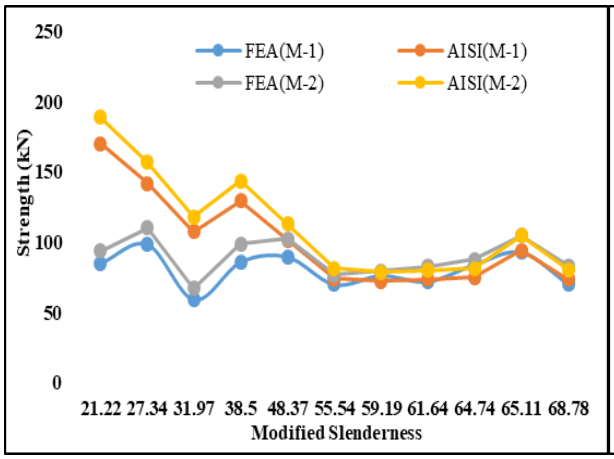

(c)

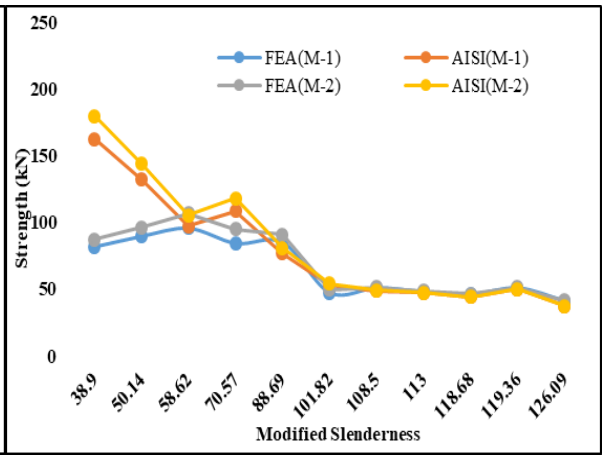

(d)

Figure 10: Strength vs slenderness ratio for (a) stub (b) short (c) intermediate (d) slender

7. CONCLUSIONS

Finite element analysis of the behavior of consecutive CFS lipped channels exposed to axial compression is the result of this research. When validating the model with test data, a nonlinear numerical analysis was done, taking into account two stress-strain curves, the entire stress-strain curve demonstrated improved congruence with test results than the simplified elastic-plastic model. The AISI code was used to compare the axial column strengths discovered by parametric study. Given that the lip height-to-thickness ratio (c/t) was taken in accordance with EC and AISI in all instances, there is strong agreement in respect to the strength values from FEM and AISI. It was observed that, in the majority of circumstances for all four types of columns, the AISI standard is rather un-conservative with regard to the practical results discovered by earlier investigators and finite element outcomes. Also, strength values are near when the breadth-to-thickness ratio is within the limit set by EC and AISI, however a considerable variation occurs when the ratio is outside the range.

REFERENCES

ABAQUS (2014), Version 6.13-1, SIMULIA, Providence, RI, USA.

American Iron Steel Institute (2016). North American specification for the design of cold formed structural members. Washington, D.C. (United States): AISI S100.

Anbarasu, M., and Ashraf, M. (2016). Behaviour and design of cold-formed lean duplex stainless steel lipped channel columns. *Thin-walled structures*, *104*, 106-115.

Anbarasu, M., Kanagarasu, K., and Sukumar, S. (2015). Investigation on the behaviour and strength of cold-formed steel web stiffened built-up battened columns. *Materials and Structures*, *48*(12), 4029-4038.

Anwar-Us-Saadat, M., Ashraf, M., and Ahmed, S. (2016). Behaviour and design of stainless steel slender cross-sections subjected to combined loading. *Thin-Walled Structures*, *104*, 225-237.

Aslani, F., and Goel, S. C. (1991). An analytical criterion for buckling strength of built-up compression members. *Eng. J*, *28*(4), 159-168.

Becque, J., Lecce, M., and Rasmussen, K. J. (2008). The direct strength method for stainless steel compression members. *Journal of Constructional Steel Research*, *64*(11), 1231-1238.

Biggs, K. A., Ramseyer, C., Ree, S., and Kang, T. H. K. (2015). Experimental testing of cold-formed built-up members in pure compression. *Steel and Composite Structures*, *18*(6), 1331-1351

Build Steel, https://buildsteel.org/why-steel/cold-formed-steel-101/what-is-cold-formed-steel-framing.

CEN, E. (2006). 1-5: 2006-Eurocode 3: Design of steel structures-Part 1-5: Plated structural elements. *Brussells: European Committee for Standardization*.

Dabaon, M., Ellobody, E., and Ramzy, K. (2015). Nonlinear behaviour of built-up cold-formed steel section battened columns. *Journal of Constructional Steel Research*, *110*, 16-28.

Darcy, G., and Mahendran, M. (2008). Development of a new cold-formed steel building system. Advances in Structural Engineering, 11(6), 661-677.

Fratamico, D. C., Torabian, S., Rasmussen, K. J., and Schafer, B. W. (2016). Experimental investigation of the effect of screw fastener spacing on the local and distortional buckling behavior of built-up cold-formed steel columns.

Gardner, L., and Nethercot, D. A. (2004). Numerical modeling of stainless steel structural components—a consistent approach. *Journal of Structural Engineering*, *130*(10), 1586-1601.

Gardner, L., and Yun, X. (2018). Description of stress-strain curves for cold-formed steels. *Construction and Building Materials*, *189*, 527-538.

Gardner, L., Saari, N., & Wang, F. (2010). Comparative experimental study of hot-rolled and cold-formed rectangular hollow sections. Thin-walled structures, 48(7), 495-507.

Kechidi, S., Fratamico, D. C., Schafer, B. W., Castro, J. M., and Bourahla, N. (2020). Simulation of screw connected built-up cold-formed steel back-to-back lipped channels under axial compression. *Engineering Structures*, *206*, 110109.

Kechidi, S., Fratamico, D. C., Schafer, B. W., Castro, J. M., and Bourahla, N. (2020). Simulation of screw connected built-up cold-formed steel back-to-back lipped channels under axial compression. *Engineering Structures*, *206*, 110109.

Lawson, R. M., Ogden, R. G., Pedreschi, R., and Popo-Ola, S. O. (2008). Developments of cold-formed steel sections in composite applications for residential buildings. *Advances in structural engineering*, *11*(6), 651-660.

Piyawat, K., Ramseyer, C., and Kang, T. H. K. (2013). Development of an axial load capacity equation for doubly symmetric built-up cold-formed sections. *Journal of Structural Engineering*, *139*(12), 04013008.

Reyes, W., and Guzmán, A. (2011). Evaluation of the slenderness ratio in built-up cold-formed box sections. *Journal of Constructional Steel Research*, *67*(6), 929-935

Roy, K., Lau, H. H., and Lim, J. B. (2019). Finite element modelling of back-to-back built-up cold-formed stainless-steel lipped channels under axial compression. Steel Compos. Struct, 33(1), 37-66.

Roy, K., Ting, T. C. H., Lau, H. H., and Lim, J. B. (2018). Experimental investigation into the behavior of back-to-back gapped built-up cold-formed steel channel sections under compression.

Roy, K., Ting, T. C. H., Lau, H. H., and Lim, J. B. (2018). Nonlinear behaviour of back-to-back gapped built-up cold-formed steel channel sections under compression. *Journal of Constructional Steel Research*, *147*, 257-276.

Roy, K., Ting, T. C. H., Lau, H. H., and Lim, J. B. (2018). Nonlinear behavior of axially loaded back-to-back built-up cold-formed steel un-lipped channel sections. *Steel and Composite Structures*, *28*(2), 233-250.

Roy, K., Ting, T. C. H., Lau, H. H., and Lim, J. B. (2018, November). Effect of thickness on the behaviour of axially loaded back-to-back cold-formed steel built-up channel sections-Experimental and numerical investigation. In *Structures* (Vol. 16, pp. 327-346). Elsevier.

Roy, K., Ting, T.C.H. Lau, H.H. and Lim, J.B.P. (2018, August). "Experimental Investigation into the Behaviour of Axially Loaded Back-to-back Cold-formed Steel Built-up Channel Sections", *Proceedings of International Conference on the* **'***Trends and Recent Advances in Civil Engineering-TRACE- 2018*', Noida, Uttar Pradesh, India.

Roy, K., Ting, T.C.H. Lau, H.H. and Lim, J.B.P. (2018, August). "Finite Element Modelling of Back-to-back Built-up Cold-formed Steel Channel Columns under Compression", *Proceedings of International Conference on the* **'***Trends and Recent Advances in Civil Engineering-TRACE-2018***'**, Noida, Uttar Pradesh, India.

Standards Australia (2005), Cold-Formed Steel Structures; AS/NZS 4600:2005, Standards Australia / Standards New Zealand.

Stone, T. A., and LaBoube, R. A. (2005). Behavior of cold-formed steel built-up I-sections. *Thin-Walled Structures*, *43*(12), 1805-1817.

Ting, T. C. H., Roy, K., Lau, H. H., and Lim, J. B. (2018). Effect of screw spacing on behavior of axially loaded back-to-back cold-formed steel built-up channel sections. *Advances in Structural Engineering*, *21*(3), 474-487.

Whittle, J., and Ramseyer, C. (2009). Buckling capacities of axially loaded, cold-formed, built-up C-channels. *Thin-Walled Structures*, *47*(2), 190-201.

Young, B., and Chen, J. (2008). Design of cold-formed steel built-up closed sections with intermediate stiffeners. *Journal of Structural Engineering*, *134*(5), 727-737.

Zhang, J. H., and Young, B. (2012). Compression tests of cold-formed steel I-shaped open sections with edge and web stiffeners. *Thin-Walled Structures*, *52*, 1-11.